Nanocellulose/chitosan biohybrid aerogel bead adsorbent for removal of diclofenac sodium from wastewater: preparation, characterization, and adsorption mechanism

Qi Tang
Sichuan Agricultural University
Chongpeng Qiu
Sichuan Agricultural University
You Zhang
Sichuan Agricultural University
Xuefeng Zhang
Mississippi State University
Zihui Yuan
Sichuan Agricultural University
Hailu Tan
Sichuan Agricultural University
Lei Wang
DATA 100 Market Research Co., Ltd
Cornelis F. Hoop
Louisiana State University Agricultural Center
Jinqiu Qi
Sichuan Agricultural University
Xingyan Huang (hxy@sicau.edu.cn)
Sichuan Agricultural University

Research Article

Keywords: Adsorption, Adsorbent, Nanocellulose, Chitosan, Diclofenac sodium

Posted Date: July 19th, 2022

DOI: https://doi.org/10.21203/rs.3.rs-1842788/v1

Nanocellulose/chitosan biohybrid aerogel bead adsorbent for removal of diclofenac sodium from wastewater: preparation, characterization, and adsorption mechanism

Qi Tang[1, 2 #], Chongpeng Qiu[1, #], You Zhang[1], Xuefeng Zhang[3], Zihui Yuan[1], Hailu Tan[1], Lei Wang[4], Cornelis F. de Hoop[5], Jinqiu Qi[1, *], Xingyan Huang[1, 2*]

1 College of Forestry, Sichuan Agricultural University, Chengdu, Sichuan, 611130, China;

2 Wood Industry and Furniture Engineering Key Laboratory of Sichuan Provincial Department of Education, Chengdu, Sichuan, 611130, China;

3 Department of Sustainable Bioproducts, Mississippi State University, MS, 39762, USA;

4 DATA 100 Market Research Co., Ltd, Beijing, 100022, China;

5 School of Renewable Natural Resources, Louisiana State University Agricultural Center, Baton Rouge, LA, 70803, USA;

Qi Tang and Chongpeng Qiu are co-first authors.

Corresponding author: hxy@sicau.edu.cn

Abstract: In this work, a novel nanocellulose/chitosan biohybrid aerogel (NCBA) bead adsorbent was successfully prepared from oxidized bamboo nanocellulose and chitosan to remove diclofenac sodium (DS) from wastewater. Fourier transform infrared spectroscopy, scanning electron microscopy, and X-ray photoelectron spectroscopy were used to characterize the preparation of NCBA bead adsorbent. The results demonstrated that the adsorption kinetics were well described by the pseudo-second-order model, and the adsorption isotherms were well fitted by the Sips isotherm model with the maximum adsorption capacity of 321.26 mg/g on DS, which

is much higher than most of the previously reported works. The absorption mechanism was governed by electrostatic interaction and hydrogen bond interaction. Moreover, the resulting bead remained a high removal efficiency after 5 regeneration cycles. In summary, it had been proved that the aerogel bead was an efficient bio-sorbent for removing DS from aqueous solutions.

Keywords: Adsorption, Adsorbent, Nanocellulose, Chitosan, Diclofenac sodium

1. Introduction

Diclofenac sodium has been a widely used nonsteroidal anti-inflammatory drug, which is commonly applied for medical purposes, such as analgesic, anti-arthritic and antirheumatic agent [1]. Owing to its broad applications, residual DS is found in groundwater and drinking water around the world [2]. Although DS can be degraded via natural and other auxiliary methods [3], residual DS in the environment is still a potential toxic contaminant. It can cause adverse gastrointestinal reactions and acute renal insufficiency [4]. Many efforts, including biodegradation [5], nanofiltration [6], adsorption [7], and photocatalysis [8], have been made to remove the residual DS in aqueous solution. Among them, adsorption is the most popular method due to its low-cost, simple operation, and reusability [7-12]. Aerogels are defined as three-dimensional networks of hydrophilic polymers, which also can be easily separated from water [13]. They have received widespread attention for DS removal because of their low density, high porosity, and high removal efficiency [14, 15].

Compared with synthetic polymer-based aerogels, the natural-based ones (such as cellulose, chitosan, and sodium alginate) are particularly attractive because of

their biodegradability, reproducibility and green preparation process [16]. Biohybrid aerogel prepared from TEMPO-oxidized cellulose and chitosan has a good performance on the adsorption of pollutants from wastewater because it can combine the advantages of cellulose and chitosan, including ample resources, renewability, and functional groups [17]. Physical cross-linking is a widely used method to produce biohybrid hydrogels *via* electrostatic attraction, hydrogen bonding, and hydrophobic interactions [18]. After freeze-drying, the physically cross-linked biohybrid aerogels will have a 3D porous network with abundant functional groups (-OH, -COOH, and $-NH_2$) [19]. Typically, the physically cross-linked biohybrid aerogels have relatively weak mechanical properties [20]. Therefore, the physically cross-linked aerogels need to be modified to improve their structural stability.

Alum is one of the most widely used coagulants to enhance the physically cross-linked aerogels in the wastewater treatment industry [21]. It will rapidly produce a great number of cationic metal species (aluminum hydroxide) after dissolving in water [22]. These cationic metal species can efficiently adsorb negatively charged contaminants. Therefore, the introduction of alum can not only enhance the stability of physically cross-linked aerogel but also improve the adsorption efficiency. γ-glycidoxypropyl trimethoxysilane (GPTMS) is a promising alkoxysilane coupling agent [23]. It will functionalize as a coupling agent to create covalently bonded compounds between chitosan and cellulose [24]. Therefore, it will enhance the graft strength of alum onto cellulose and chitosan. Meanwhile, it also enhances the mechanical strength of physically cross-linked aerogels [25].

Biohybrid aerogels usually have tunable surface characteristics through surface modification, which makes them more capable of absorb pollutants [26]. Polyethyleneimine (PEI), a hydrosoluble cationic polyelectrolyte, has been recognized by its abundant amino groups [3]. Meanwhile, it has been extensively used to adsorb dyes [27], heavy metal ions [28], and pharmaceutical residues [29]. Thus, PEI can be used as an amino-functionalized agent to boost the adsorption performance of biohybrid aerogel towards DS.

Herein, with the aim of efficiently removing DS from wastewater, a nanocellulose/chitosan biohybrid aerogel (NCBA) bead adsorbent was prepared from waste bamboo paper and chitosan. The NCBA bead was characterized by FTIR, XPS, and SEM. In addition, these vital factors that influence the adsorption properties of NCBA bead were investigated and the DS removal mechanisms were studied as well.

2. Material and methods

2.1 Materials

Waste bamboo paper was collected from the laboratory. Glacial acetic acid, polyethyleneimine (PEI), γ-glycidyloxypropyl trimethoxysilane (GPTMS), chitosan (CS), and diclofenac sodium (DS) were purchased from Aladdin Chemical Reagent Co. Ltd. (Shanghai, China). All chemicals were used as received.

2.2 Preparation of CNF-Alum

The oxidized bamboo nanocellulose (CNF) was prepared according to our previous work [17]. Oxidized CNF (0.5 g) was dissolved in 50 mL distilled water. The suspension was then sonicated for 10 min. Then, GPTMS (400 μL) was added to

the solution and subsequently, the solution was stirred at 60ºC for 0.5 h. After the reaction was completed, the solution was mixed with 0.25 g alum under stirring for 1 h to prepare CNF-Alum.

2.3 Preparation of NCBA bead

The CNF-Alum (50 mL) suspension was mixed with acetic acid (1 mL) under constant stirring at 60 ºC for 20 min. Then, the CNF-Alum suspension was mixed with 1 g CS. The CNF-Alum@CS suspension was stirred rapidly at 50 ºC until a homogeneous mixture was obtained. The CNF-Alum@CS suspension was dropwise added into a precipitation bath (1 M NaOH) to form CNF-Alum@CS bead. The obtained bead was washed with deionized water. Then, it was mixed with deionized water (200 mL) and PEI (2 g) at 50 ºC for 6 h to produce an amino-functionalized nanocellulose/chitosan biohybrid aerogel (NCBA) bead, and then the resulting bead was freeze-dried for 48 h. The synthetic procedure of NCBA bead is shown in **Fig. 1.**

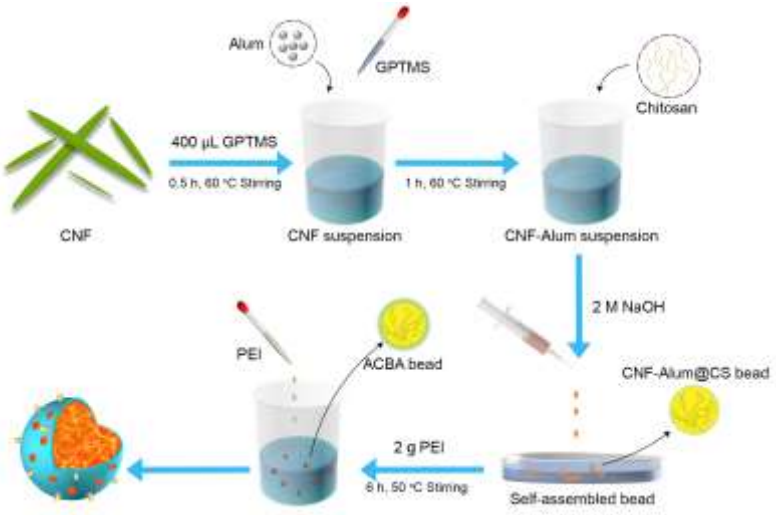

Fig. 1. Synthetic procedure of NCBA bead.

2.4 Characterization

105 The morphology of NCBA bead was carried out by scanning electron
106 microscopy (SEM, ZEISS Gemini 300). The chemical structure of NCBA bead was
107 characterized by Fourier-transform infrared spectroscopy (FTIR, Nicolet 670), and
108 X-ray photoelectron spectroscopy (XPS, Thermo Scientific K-Alpha). The point of
109 zero charge (pH_{PZC}) of NCBA bead was measured according to the pH drift method
110 [17].

111 **2.5 Adsorption and desorption experiments**

112 The adsorption experiments were performed by placing 50 mg NCBA bead in a
113 series of vials containing 50 mL DS solution with desired concentration. After
114 shaking the solution at 180 rpm at 25 ^{o}C for a predefined time. The residual DS
115 concentration was measured by UV-vis spectrometer at the DS maximum adsorption
116 wavelength of 276 nm. The effect of initial DS concentration on the adsorption was
117 investigated from 50 to 800 mg/L. The effect of contact time was carried out with
118 adsorption time from 0 to 240 min. All tests were conducted in triplicate. The
119 adsorption capacity (q_e, mg/g) and removal ratio (R, %) were calculated as follows:

120 $$q_e = \frac{C_0 - C_e}{m} V \quad (1)$$

121 $$R = \frac{C_0 - C_e}{C_0} \times 100 \quad (2)$$

122 where: q_e (mg/g), C_0 (mg/L), C_e (mg/L), m (mg), and V (mL) are adsorption capacity,
123 the initial and equilibrium concentrations, adsorbent dosage and solution volume,
124 respectively.

125 Desorption experiments were performed as follows. The initial DS concentration,
126 solution pH, and adsorbent dose were 100 mg/L, 5.2, and 1 g/L, respectively. After 24

h adsorption, the residual concentration of DS was measured. The NCBA bead was soaked in NaOH solution (0.5 mol/L) for 4 h, followed by vacuum-dried at 60 ^{o}C for the next cycle. It was repeated 5 times to study its reusability.

3. Results and discussion

3.1 Characterization of NCBA bead

3.1.1 SEM analysis

As shown in **Fig. 2a**, the surface of CNF was covered by alum, which exhibited a loose surface structure of CNF-Alum, suggesting the successful grating of alum onto CNF [30]. Interestingly, a smoother surface of CNF-Alum@CS bead was formed after introducing CS (**Fig. 2b**), which may be ascribed to the strong inter-hydrogen and intra-hydrogen bond forces [31]. In addition, a rough bead surface with irregular pores could be observed on NCBA bead after involving in PEI (**Fig. 2c** and **d**), which was expected to have a large specific area. This structure was benefit to providing more accessible adsorption sites for DS.

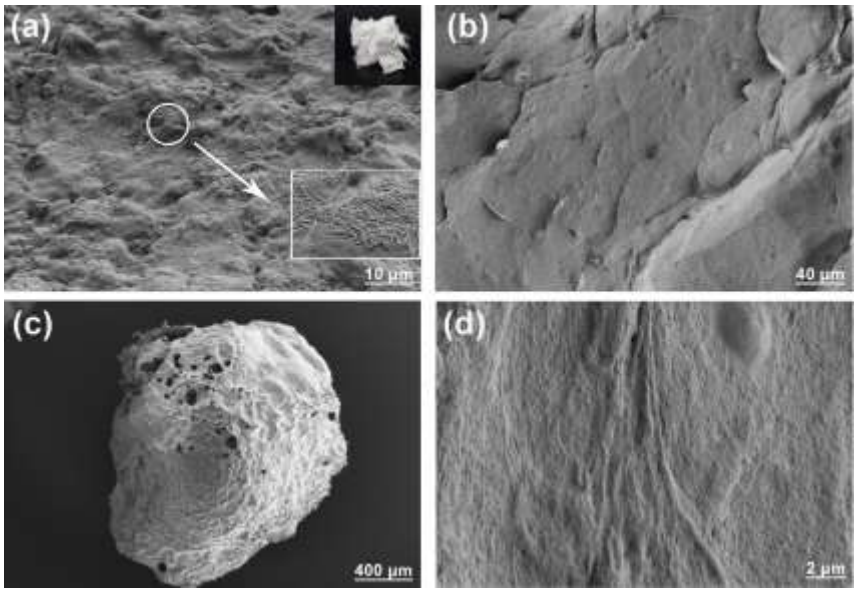

Fig. 2. SEM images of (a) CNF-Alum; (b) CNF-Alum@CS; (c-d) NCBA bead.

3.1.2 FTIR analysis

Fig. 3 shows the FTIR spectra of CNF-Alum, CNF-Alum@CS, and NCBA bead. It was observed that the CNF-Alum had characteristic peaks at 3440, 1720, 1610, and 897 cm^{-1}, which associated with the symmetry vibrations of -OH, C=O, C-OH, and glucosidic ring, respectively. Additionally, the existence of three adsorption peaks at 1050, 634, and 475 cm^{-1} were assigned as asymmetric stretch vibrations from Si-O-Al and Si-O-Si [32]. It indicated that the alum was successfully grafted on the oxidized bamboo nanocellulose *via* cross-linking with GPTMS. In the spectrum of CNF-Alum@CS, the characteristic peaks at 1650, 1520, and 1230 cm^{-1} were attributed to the stretching vibration of C=C and C=O, which evidenced the introduction of CS [33, 34]. As compared with CNF-Alum@CS, the band at 1600 cm^{-1} was weakened in NCBA bead, which may be ascribed to the Schiff base reaction with grafting PEI [35]. It was noted that the N-C-N asymmetric stretching at 1453 cm^{-1} was observed in the NCBA bead. It was also confirmed that the PEI (amino-functionalization) was successfully grafted onto the surface of CNF-Alum@CS [36].

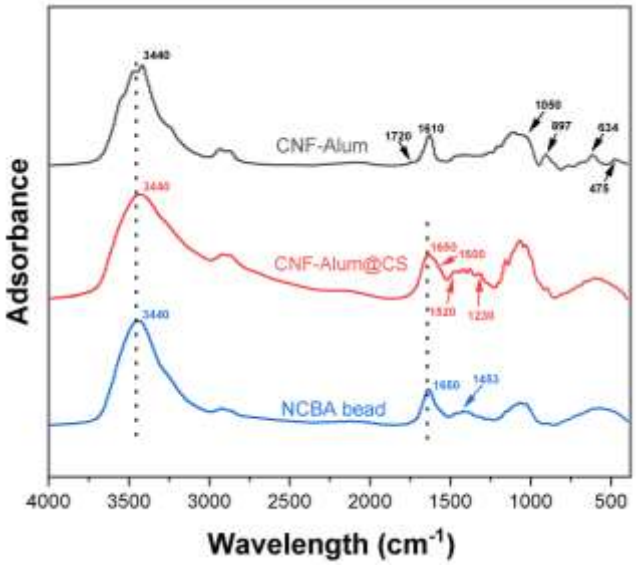

Fig. 3. FTIR spectra of CNF-Alum, CNF-Alum@CS, and NCBA bead.

3.1.3 XPS analysis

The XPS spectra of CNF-Alum, CNF-Alum@CS, and NCBA bead were recorded to investigate the element states on their surfaces. As shown in **Fig.4a**, the peaks at 101.8, 286.08, 399.08, and 532.08 eV were related to Si2p, C1s, N1s and O1s electrons, respectively. As compared with CNF-Alum, the intensities of C1s and O1s were significantly increased in the NCBA bead. In addition, a new peak of N1s was observed in CNF-Alum@CS, while the peak of Si2p disappeared in CNF-Alum. These results suggested that CNF-Alum was covered by CS [37]. For NCBA bead, peaks at 284.88, 285.88, 287.48, and 288.18 eV in the high-resolution C1s spectrum (**Fig. 4b)** were attributed to C=C/C-C, C-O, C-N, and C=O, respectively [28]. This observation was in agreement with the FTIR results and confirmed the grafting of PEI onto CNF-Alum@CS. Two peaks ascribed to $-NH_2$ (399.75 eV) and $-NH_3^+$ (401.08 eV) were observed in the high-resolution N1s spectrum of the NCBA bead (**Fig. 4c**), indicating the abundance of amino groups that resulted from the introduction of $-NH_2$

from CS and PEI [38]. In the O1s spectrum (**Fig. 4d)**, three peaks at 530.94, 532.36, and 533.51 eV corresponded to O-H, O-C, and O=C, respectively [28]. It demonstrated the abundant carboxyl groups and hydroxyl groups of NCBA bead. These results further indicated that the physical cross-linking included electrostatic attraction ($-COO^-$ and $-NH_3^+$) and hydrogen bonding (-OH groups) [39]. As shown in **Fig. 4e,** the peaks at 102.08 and 101.68 eV were associated with Si-O-C and Si-O-Al, respectively, proving that the alum was successfully grafted on oxidized bamboo nanocellulose *via* cross-linking with GPTMS. The peak of Si-O-Al was mainly due to the reaction between $Si\text{-}OC_2H_5$ or Si-OH and -OH in alum when dissolving in water [40].

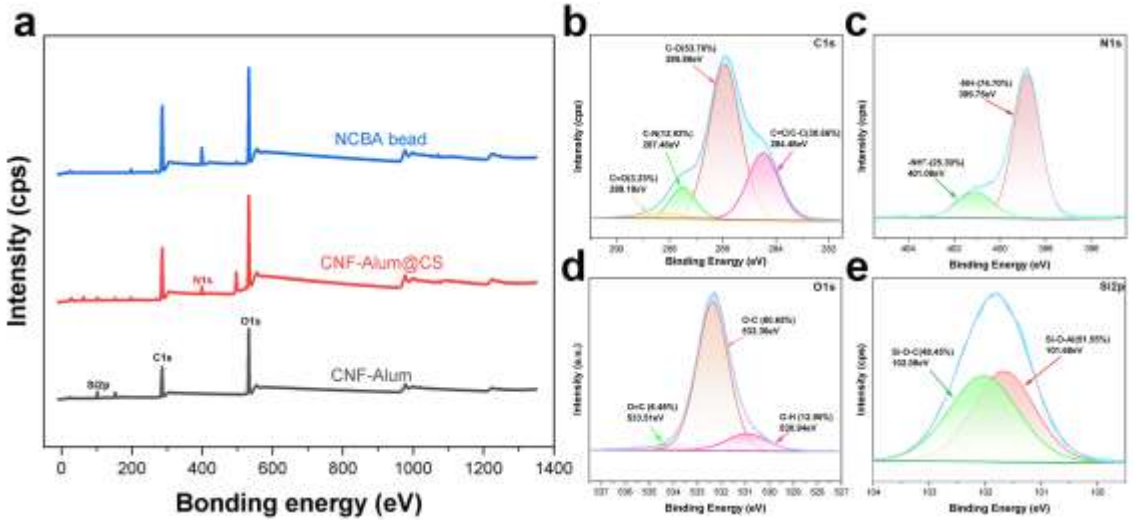

Fig. 4. (a) High-resolution XPS spectra of CNF-Alum, CNF-Alum@CS, and NCBA bead; high-resolution XPS spectra of (b) C1s, (c) N1s, (d) O1s, and (e) Si2p of NCBA bead.

3.2 Adsorption and desorption of DS

3.2.1 Effect of initial pH

The solution pH is an essential parameter in water remediation by adsorption. The point of zero charge (pH_{PZC}) is an independent model to characterize the surface

charge of adsorbent in an aqueous solution. The pH_{PZC} of NCBA bead was 6.42, as shown in **Fig. 5a**. It indicated that the surface of NCBA bead was negatively charged at the solution pH > 6.42, while its surface was positively charged at the solution pH < 6.42. Therefore, the electrostatic attraction between diclofenac anions and the NCBA bead is promoted at low pH solutions.

The adsorption capacity of DS was decreased from 49.17 to 20.15 mg/g and DS removal efficiency decreased from 98.31% to 50.08% with increasing solution pH from 4 to 10 (**Fig. 5b**). This was expected because the deprotonation of the amino ($-NH_2$) and carboxyl ($-COO^-$) groups resulted in a negatively charged NCBA bead surface that induced the electrostatic repulsion between the NCBA bead and diclofenac anions, thereby reducing the diclofenac uptake [7].

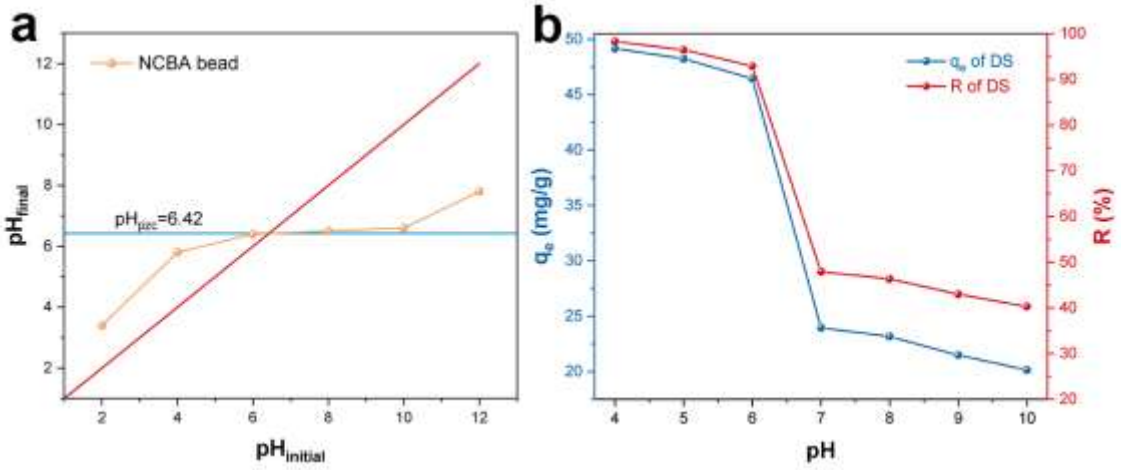

Fig. 5. (a) Zero point position; (b) The effect of pH on DS solution.

3.2.2 Adsorption kinetics

As shown in **Fig.6**, the adsorption capacity was very fast within the first 60 min. Then, it slowed down until reaching the equilibrium at 240 min. The DS removal efficiency increased from 22.65% to 70.30% by prolonging the contact time. It was

ascribed to the available adsorption sites in NCBA bead. They were gradually occupied with prolonging contact time.

In order to study the adsorption process, the kinetic experimental data of DS adsorption by NCBA bead were fitted using pseudo-first-order and pseudo-second-order models [34, 41]. The corresponding equations were shown as follows:

Pseudo-first-order equation: $ln(q_e - q_t) = ln\, q_e - k_1 t$ (3)

Pseudo-second-order equation: $\frac{t}{q_t} = \frac{1}{k_2 q_e^{\,2}} + \frac{t}{q_e}$ (4)

where q_e (mg/g) and q_t (mg/g) represent the adsorbate uptakes at equilibrium and time t (min), respectively. k_1 (1/min) and k_2 (g/(mg, min) are the pseudo-first-order and pseudo-second-order rate constant, respectively.

Fig.6 and **Table 1** show the fitting curves and parameters, respectively. The correlation coefficient (R^2=0.9897) of pseudo-second-order kinetic model was higher than that of pseudo-first-order kinetic model. Additionally, the q_e (135.82 mg/g) calculated from pseudo-second-order kinetic model was in good agreement with the experimental data (140.60 mg/g). These findings indicated that the adsorption process of DS was well described by the pseudo-second-order kinetic model. This model suggested that the adsorption process of DS was mainly controlled by chemical adsorption involving electron exchange between DS and adsorbent [41].

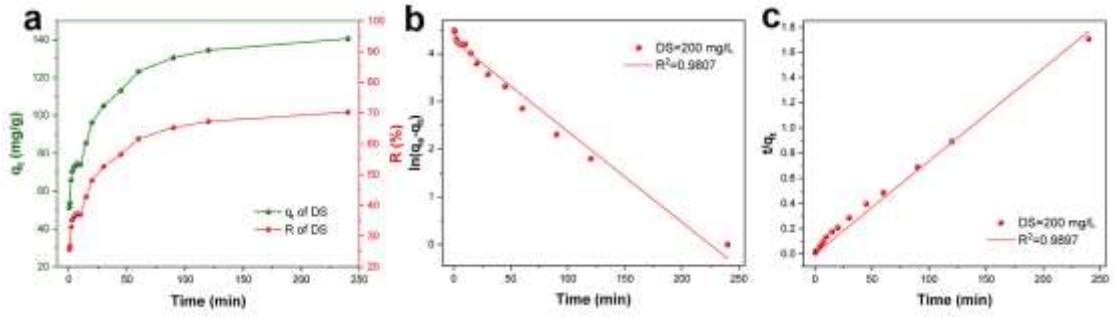

Fig. 6. (a) Effect of contact time on DS uptake; (b) Linear plots of pseudo-first-order for DS uptake; (c) Linear plots of pseudo-second-order model for DS adsorption.

Table 1 Kinetic parameters for the adsorption of DS by NCBA bead.

Isotherm models	Parameters	Adsorbate DS
Pseudo-first-order	q_e	71.8093
	k_1	0.0190
	R^2	0.9807
Pseudo-second-order	q_e	135.8229
	k_2	-0.0005
	R^2	0.9897

3.2.3 Adsorption isotherms

The concentration-dependent adsorption of DS by NCBA bead was studied with an initial concentration from 50 to 800 mg/L at 25 ºC (pH= 5.0). As shown in **Fig. 7**, the adsorption capacity was increased with increasing initial DS concentration. It could be ascribed to the increase of mass driving force when the initial DS concentration increased [45].

Adsorption isotherms are widely applied to describe the adsorption behavior. The equilibrium data were evaluated by the Langmuir, Freundlich, and Sips isotherm models [43, 44]. The corresponding equations were expressed as follows:

Langmuir equation: $$\frac{C_e}{q_e} = \frac{1}{bq_m} + \frac{C_e}{q_m} \quad (5)$$

Freundlich equation: $$\log q_e = \log K_F + \frac{1}{n}\log C_e \quad (6)$$

Sips equation: $$q_e = \frac{q_m (k_s C_e)^{\gamma}}{1+(k_s C_e)^{\gamma}} \quad (7)$$

where q_m is the maximum adsorption capacity, $1/n$ and $1/b$ are the Langmuir and Freundlich constants, respectively, and K_F is a constant representing the adsorption capacity. K_S is the Sips constant, and γ represents the surface inhomogeneity of the adsorbent.

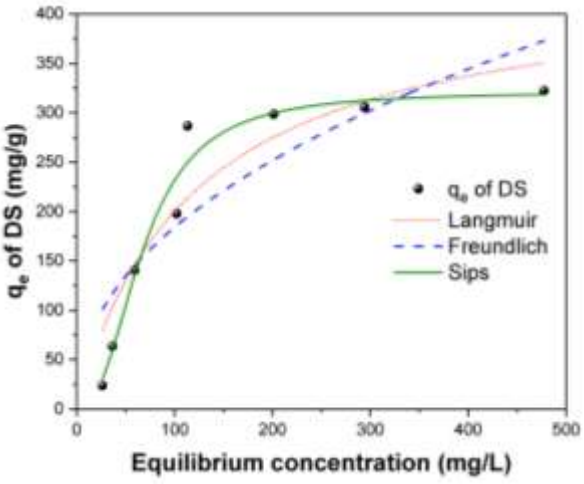

Fig. 7. Isotherm plots for the adsorption of DS by NCBA bead.

Table 2 Isotherm parameters for the adsorption of DS by NCBA bead.

Isotherm models	Parameters	Adsorbate DS
Langmuir	k	0.0085
	q_m	437.0703
	R^2	0.8818
Freundlich	K_F	22.9980
	n	2.2140
	R^2	0.7708
Sips	q_m	321.2583
	K_S	0.0387
	R^2	0.9702

The fitting results are shown in **Fig. 7**, and the fitting data are given in **Table 2**. The R^2 value (0.9702) calculated from the Sips isotherm model was much higher than

other models (**Table 2**), indicating that the Sips isotherm described well the adsorption of DS by NCBA bead. This model indicated that the adsorption process of DS was followed by a combined model: monomolecular (at high DS concentration) and diffuse (at low DS concentrations) [46]. The maximum adsorption capacity obtained from the Sips isotherm model was 321.26 mg/g for DS, which was higher than most of the previously reported works (**Table 3**).

Table 3 Comparison of the maximum DS adsorption capacity by various adsorbents.

Adsorbents	q_{max} (mg/g)	Adsorption time (min)	Ref.
Chitosan-based magnetic composite	196.00	720	[38]
CNC-ED@CS-ED	444.44	50	[29]
rGO	56.67	200	[2]
Zeolitic−CTAB	60.58	90	[47]
Fe_3O_4@SiO_2/SiHTCC	240.40	300	[45]
Carbon xerogels	182.50	2880	[48]
$(PAA/PEI)_{25}$	32.42	120	[49]
NCBA bead	321.26	240	This work

3.2.4 Reusability of adsorbents

To evaluate the regeneration property of the NCBA bead, five adsorption-desorption cycle experiments were carried out using NaOH as eluent. The removal efficiency remained above 50% after five adsorption-desorption processes

(**Fig. 8**), indicating that it had excellent reusability. The adsorption capacity was decreased from 153.82 to 103.74 mg/g after five cycles. It was probably attributed to the loss weight of adsorbent during the recycling process [50].

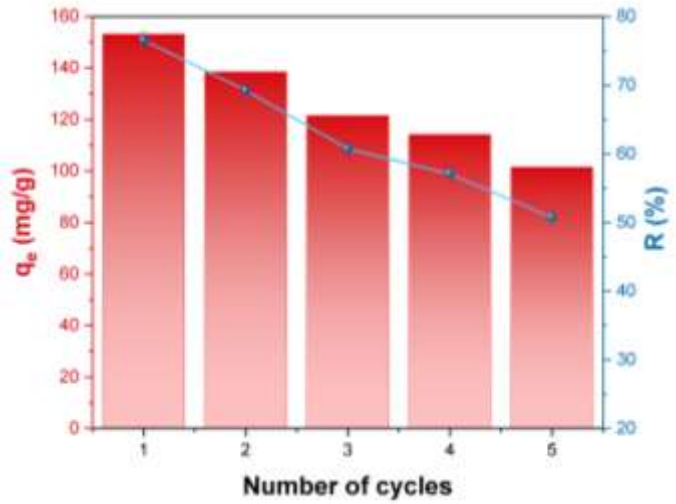

Fig. 8. Five cycles of DS adsorption and desorption.

3.3 Adsorption mechanism study

FTIR spectra of NCBA bead before and after DS adsorption are shown in **Fig. 9**. After adsorbing DS, the characteristic peak of hydroxyl groups was red-shifted to 3420 cm^{-1} and its intensity was decreased, indicating that the hydrogen bonding was involved in DS adsorption process. The bands at 1520, 1230, and 750 cm^{-1} were assigned to the stretching vibration of C=O and C-Cl in DS [51]. After adsorption, these characteristic peaks appeared in NCBA bead@DS, suggesting successful DS adsorption.

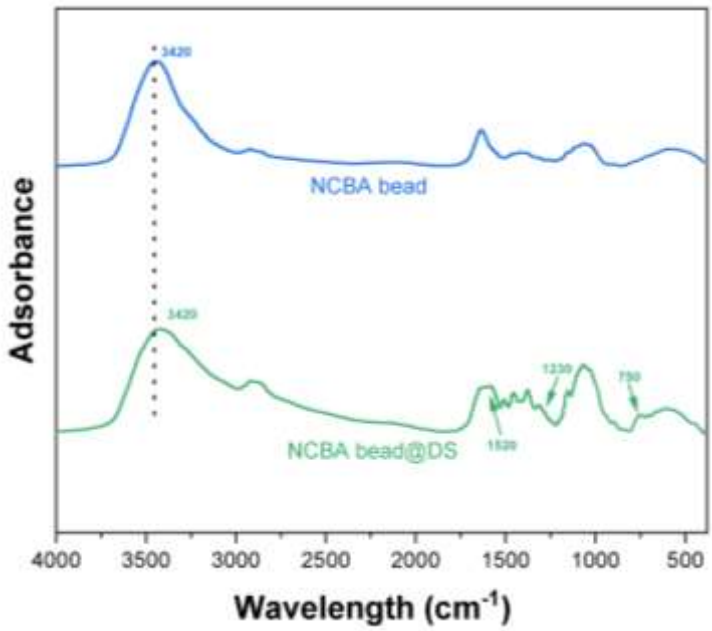

Fig. 9. The FTIR of NCBA bead before and after adsorption DS.

XPS results are presented in **Fig. 10**. After absorbing DS, the intensities of C1s and O1s were slightly decreased in NCBA bead@DS, and both of them shifted to lower binding energy. Besides, a new peak of Cl2p was found in NCBA bead@DS. These results indicated successful DS adsorption [51]. As shown in **Fig. 10b**, the N1s spectrum was divided into two peaks, corresponding to $-NH_2$ and protonated $-NH_3^+$, respectively. After DS adsorption, the $-NH_3^+$ increased, while the $-NH_2$ decreased (**Fig. 10c**). It was probably due to the electrostatic attraction between $-NH_3^+$ and DS [29]. **Fig. 10d** displayed that the C1s spectrum consisted of four components, which were associated with C=O, C-N, C-O, and C=C/C-C, respectively. After DS adsorption, the C=O and C-O peaks were shifted to lower binding energies, indicating that the adsorption of DS was triumphant [51]. A new characteristic peak C-Cl could be seen in C1s spectrum (**Fig. 10e**). The Cl element was the characteristic element in DS, also confirming the successful DS adsorption [52].

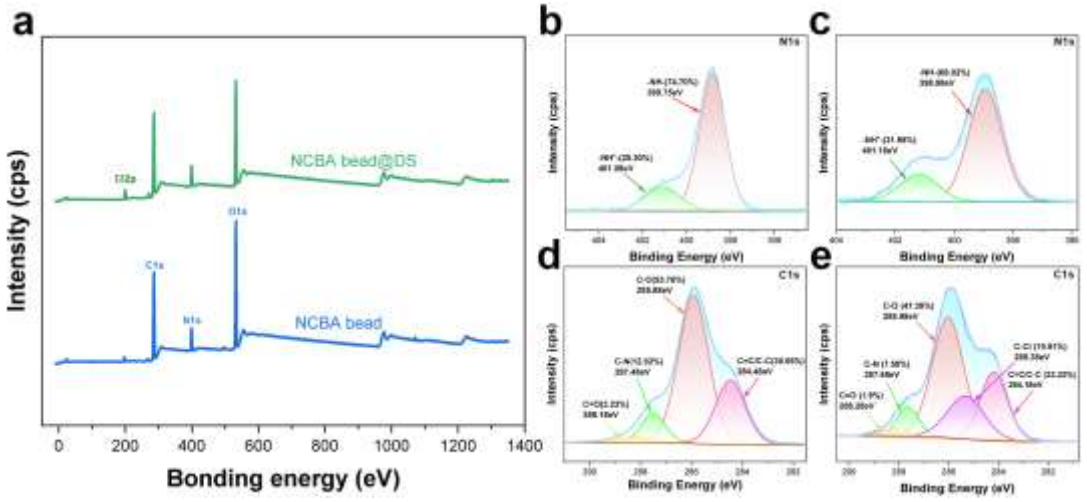

Fig. 10. (a) High-resolution XPS spectra of NCBA bead before and after adsorption; (b) N1s and (d) C1s before adsorption; (c) N1s and (e) C1s after adsorption.

The DS adsorption mechanism was proposed in **Fig. 11**. At solution pH= 4.20-6.42, the amino groups on the NCBA bead surface were protonated ($-NH_3^+$) acquiring positive charges, which favored electrostatic attraction with the groups of DS. In addition, the hydrogen bonding between -OH groups (oxidized bamboo nanocellulose, $Al(OH)_3$, GPTMS, and CS) and deprotonated DS had a positive contribution to the DS adsorption. At solution pH > 6.42, the removal mechanism was the DS interaction with hydroxyl groups on the surface of the NCBA bead.

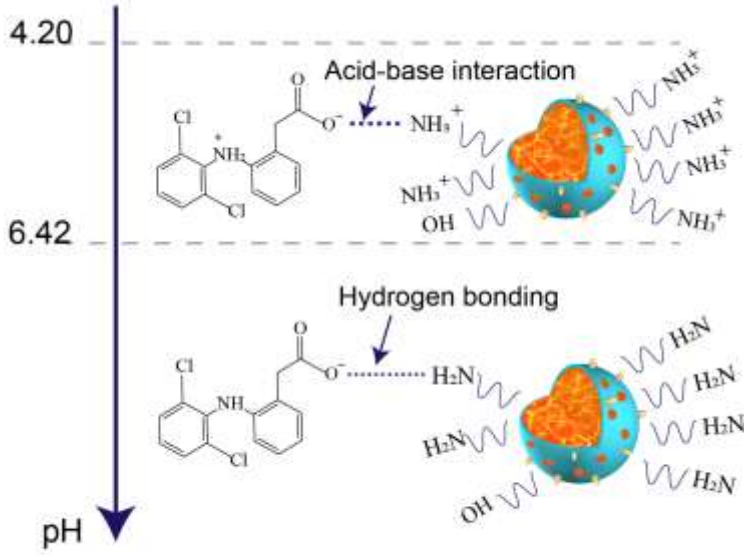

Fig. 11. Proposed schematic diagram of DS adsorption mechanism by NCBA bead.

4. Conclusion

In this study, a nanocellulose/chitosan biohybrid aerogel (NCBA) bead adsorbent was prepared for removing DS from aqueous solutions. The point of zero charge (pH_{PZC}) obtained from the pH drift method was 6.42. The adsorption of DS was fitted well by pseudo-second-order kinetic model, suggesting the involvement of chemical adsorption. The adsorption process of DS was well described by the Sips isotherm model. The maximum adsorption capacity for DS was evaluated as 321.26 mg/g according to the Sips isotherm model. Additionally, the absorption mechanism was governed by electrostatic interaction and hydrogen bond interaction. This study indicated that the NCBA bead had a great potential application for DS wastewater purification.

Declaration of Competing Interest

The authors declare that they have no known competing financial interests or

personal relations that have appeared to influence the work reported in this paper.

Acknowledgment

The authors would like to thank the National Natural Science Foundation of China (32101598). Dr. Xuefeng Zhang acknowledges the support from Forest and Wildlife Research Center, Mississippi State University.

References

[1] Nassef M, Matsumoto S, Seki M, Khalil F, Kang IJ, Shimasaki Y, Honjo T (2010) Acute effects of triclosan, diclofenac and carbamazepine on feeding performance of Japanese medaka fish (Oryzias latipes). Chemosphere 80(9):1095-1100

[2] Jauris IM, Matos CF, Saucier C, Lima EC, Zarbin AJG, Fagan SB, Machado, FM, Zanella I (2016) Adsorption of sodium diclofenac on graphene: a combined experimental and theoretical study.Phys. Chem. Chem. Phys 18(3):1526-1536

[3] Li J, Huang X, Hou Z, Ding T (2022) Sorption of diclofenac by polystyrene microplastics: Kinetics, isotherms and particle size effects. Chemosphere 290:133311

[4] Nassef M, Matsumoto S, Seki M, Khalil F, Kang IJ, Shimasaki Y, Honjo T (2010) Acute effects of triclosan, diclofenac and carbamazepine on feeding performance of Japanese medaka fish (Oryzias latipes). Chemosphere 80(9):1095-1100

[5] Moradi O, Alizadeh H, Sedaghat S (2022) Removal of pharmaceuticals (diclofenac and amoxicillin) by maltodextrin/reduced graphene and maltodextrin/reduced graphene/copper oxide nanocomposites. Chemosphere 299:134435

339 [6] Egea-Corbacho A, Ruiz SG, Alonso JMQ (2019) Removal of emerging contaminants from
340 wastewater using nanofiltration for its subsequent reuse: Full-scale pilot plant. J. Cleaner Prod
341 214:514-523
342 [7] Mao S, Bao R, Fang D, Yi J (2019) Fabrication of sliver/graphitic carbon nitride photocatalyst with
343 enhanced visible-light photocatalytic efficiency through ultrasonic spray atomization. J. Colloid
344 Interface Sci 538:15-24
345 [8] Garcia JJM, Nuñez JAP, Salapare III HS, Vasquez Jr MR (2019) Adsorption of diclofenac sodium
346 in aqueous solution using plasma-activated natural zeolites. Results Phys 15:102629
347 [9] Liang X, Omer A, Hu Z, Wang Y, Yu D, Ouyang X (2019) Efficient adsorption of diclofenac
348 sodium from aqueous solutions using magnetic amine-functionalized chitosan. Chemosphere
349 217:270-278
350 [10] Truong HB, Bae S, Cho J, Hur J (2022) Advances in application of g–C_3N_4–based materials for
351 treatment of polluted water and wastewater via activation of oxidants and photoelectrocatalysis: A
352 comprehensive review. Chemosphere 286:131737
353 [11] Ali I (2018) Microwave-assisted the economic synthesis of multi-walled carbon nanotubes for
354 arsenic species removal in water: Batch and column operations. J. Mol. Liq 271:677-685
355 [12] Ma J, Xia M, Zhu S, Wang F (2020) A new alendronate doped HAP nanomaterial for Pb^{2+}, Cu^{2+}
356 and Cd^{2+} effect absorption. J. Hazard. Mater 400:123143
357 [13] Lv Y, Liang Z, Li Y, Chen Y. Liu K, Yang G, Liu M (2021) Efficient adsorption of diclofenac
358 sodium in water by a novel functionalized cellulose aerogel. Environ. Res 194:110652
359 [14] Wan C, Jiao Y, Wei S, Zhang L, Wu Y, Li J (2019) Functional nanocomposites from sustainable
360 regenerated cellulose aerogels: a review. Chem. Eng. J 359:459-475

[15] Aaltonen O, Jauhiainen, O (2009) The preparation of lignocellulosic aerogels from ionic liquidsolutions. Carbohydr. Polym 75(1):125-129

[16] Sionkowska A (2011) Current research on the blends of natural and synthetic polymers as new biomaterials. Prog. Polym. Sci 36(9):1254-1276

[17] Qiu C, Tang Q, Zhang X, Li MC, Zhang X, Xie J, Huang X (2022) High-efficient double-cross-linked biohybrid aerogel biosorbent prepared from waste bamboo paper and chitosan for wastewater purification. J. Cleaner Prod 338:130550

[18] Ji J, Xiong H, Zhu Z, Li L, Huang Y, Yu X (2018) Fabrication of polypyrrole/chitosan nanocomposite aerogel monolith for removal of Cr (VI). J. Polym. Environ 26(5):1979-1985

[19] Jan J, Chen P, Hsieh PL, Chen B (2012) Silicification of genipin-cross-linked polypeptide hydrogels toward biohybrid materials and mesoporous oxides. ACS Appl. Mater Interfaces 4(12):6865-6874

[20] Madyan OA, Fan M, Feo L, Hui D (2016) Enhancing mechanical properties of clay aerogel composites: An overview. Composites, Part B 98:314-329

[21] Majhi D, Patra BN (2018) Preferential and enhanced adsorption of dyes on alum doped nanopolyaniline. J. Chem. Eng. Data 63(9):3427-3437

[22] Patra BN, Majhi D (2015) Removal of anionic dyes from water by potash alum doped polyaniline: investigation of kinetics and thermodynamic parameters of adsorption. J. Chem. Phys B 119(25):8154-8164

[23] Cheng H, Li Y, Wang B, Mao Z, Xu H, Zhang L, Zhong Y, Sui X (2018) Chemical crosslinking reinforced flexible cellulose nanofiber-supported cryogel. Cellulose 25(1):573-582

382 [24] Tonda-Turo C, Gentile P, Saracino S, Chiono V, Nandagiri VK, Muzio G, Ciardelli G (2011)
383 Comparative analysis of gelatin scaffolds crosslinked by genipin and silane coupling agent. Int. J.
384 Biol. Macromol 49(4):700-706
385 [25] Wu M, Chen X, Xu J, Zhang H (2022) Freeze-thaw and solvent-exchange strategy to generate
386 physically cross-linked organogels and hydrogels of curdlan with tunable mechanical properties.
387 Carbohydr. Polym 278:119003
388 [26] Mohamed MA, Abd Mutalib M, Hir ZAM, Zain MFM, Mohamad AB, Minggu LJ, Awang NA,
389 Salleh WNW (2017) An overview on cellulose-based material in tailoring bio-hybrid
390 nanostructured photocatalysts for water treatment and renewable energy applications. Int. J. Biol.
391 Macromol 103:1232-1256
392 [27] Zhang Y, Zhang Y, Wang Q, Fan X (2017) Preparation and properties of a chitosan−hyaluronic
393 acid-polypyrrole conductive hydrogel catalyzed by laccase. J. Polym. Environ 25(3):526-532
394 [28] Liu C, Jin R, Ouyang X, Wang Y (2017) Adsorption behavior of carboxylated cellulose
395 nanocrystal—polyethyleneimine composite for removal of Cr (VI) ions. Appl. Surf. Sci
396 408:77-87
397 [29] Hu D, Jiang R, Wang N, Xu H, Wang Y, Ouyang X (2019) Adsorption of diclofenac sodium on
398 bilayer amino-functionalized cellulose nanocrystals/chitosan composite. J. Hazard. Mater
399 369:483-493
400 [30] Ghorbani F, Zamanian A, Behnamghader A, Daliri Joupari M (2018) A novel pathway for in situ
401 synthesis of modifified gelatin microspheres by silane coupling agents as a bioactive platform. J.
402 Appl. Polym. Sci 135(41):46739

[31] Wang N, Ouyang X, Yang L, Omer AM (2017) Fabrication of a magnetic cellulose nanocrystal/metal-organic framework composite for removal of Pb (II) from water. ACS Sustainable Chem. Eng 5(11):10447-10458

[32] Rachman RA, Martia UTI, Aulia W, Iqbal RM, Widiastuti N, Kurniawan F (2018) Combination of microbial fuel cell and zeolite Na-Y adsorption for chromium removal. AIP Conf. Proc 2049(1):020073

[33] Zhang J, Ma J, Zhang S, Wang W, Chen Z (2015) A highly sensitive nonenzymatic glucose sensor based on CuO nanoparticles decorated carbon spheres. Sens. Actuators B Chem 211:385-391

[34] Katal R, Hasani E, Farnam M, Baei MS, Ghayyem MA (2012) Charcoal ash as an adsorbent for Ni (II) adsorption and its application for wastewater treatment. J. Chem. Eng. Data 57(2):374-383

[35] Zhang W, Deng Q, He Q, Song J, Zhang S, Wang H, Zhang H (2018) A facile synthesis of core-shell/bead-like poly (vinyl alcohol)/alginate@PAM with good adsorption capacity, high adaptability and stability towards Cu (II) removal. Chem. Eng. J 351:462-472

[36] Lu B, Lin Q, Yin Z, Lin F, Chen X, Huang B (2021) Robust and lightweight biofoam based on cellulose nanofibrils for high-efficient methylene blue adsorption. Cellulose 28(1):273-288

[37] Sun K, Shi Y, Chen H, Wang X, Li Z (2017) Extending surfactant-modified 2: 1 clay minerals for the uptake and removal of diclofenac from water. J. Hazard. Mater 323:567-574.4

[38] Zhang S, Dong Y, Yang Z, Yang W, Wu J, Dong C (2016) Adsorption of pharmaceuticals on chitosan-based magnetic composite particles with core-brush topology. Chem. Eng. J 304:325-334

[39] Lowe B, Venkatesan J, Anil S, Shim MS, Kim SK (2016) Preparation and characterization of chitosan-natural nano hydroxyapatite-fucoidan nanocomposites for bone tissue engineering. Int. J. Biol. Macromol 93:1479-1487

[40] Zhou W, Wu P, Zhang L, Zhu D, Zhao X, Cai Y (2022) Heavy metal ions and particulate pollutants can be effectively removed by a gravity-driven ceramic foam filter optimized by carbon nanotube implantation. J. Hazard. Mater 421:126721

[41] Paraskar PM, Kulkarni RD (2021) Synthesis of isostearic acid/dimer fatty acid-based polyesteramide polyol for the development of green polyurethane coatings. J. Polym. Environ 29(1):54-70

[42] Xiong T, Yuan X, Wang H, Wu Z, Jiang L, Leng L, Xi K, Cao X, Zeng G (2019) Highly efficient removal of diclofenac sodium from medical wastewater by Mg/Al layered double hydroxide-poly (m-phenylenediamine) composite. Chem. Eng. J 366:83-91

[43] Deng S, Ting YP (2005) Fungal biomass with grafted poly (acrylic acid) for enhancement of Cu (II) and Cd (II) biosorption, Langmuir 21(13):5940-5948

[44] Weng X, Ma L, Guo M, Su Y, Dharmarajan R, Chen Z (2018) Removal of doxorubicin hydrochloride using Fe3O4 nanoparticles synthesized by euphorbia cochinchinensis extract, Chem. Eng. J 353:482-489

[45] Soares SF, Fernandes T, Sacramento M, Trindade T, Daniel-da-Silva AL (2019) Magnetic quaternary chitosan hybrid nanoparticles for the efficient uptake of diclofenac from water. Carbohydr. Polym 203:35-44

[46] Ahmed MJK, Ahmaruzzaman M (2015) A facile synthesis of Fe_3O_4-charcoal composite for the sorption of a hazardous dye from aquatic environment. J. Environ. Manage 163:163-173

[47] Lin K, Yang H, Lee WD (2015) Enhanced removal of diclofenac from water using a zeolitic imidazole framework functionalized with cetyltrimethylammonium bromide (CTAB). RSC Adv 5(99):81330-81340

[48] Álvarez S, Ribeiro RS, Gomes HT, Sotelo JL, García J (2015) Synthesis of carbon xerogels and their application in adsorption studies of caffeine and diclofenac as emerging contaminants. Chem. Eng. Res. Des 95:229-238

[49] Ghiorghita CA, Bucatariu F, Dragan ES (2016) Sorption/release of diclofenac sodium in/from free-standing poly (acrylic acid)/poly (ethyleneimine) multilayer films. J. Appl. Polym. Sci 133(31):43752

[50] Zhu S, Khan MA, Wang F, Bano Z, Xia M (2020) Rapid removal of toxic metals Cu^{2+} and Pb^{2+} by amino trimethylene phosphonic acid intercalated layered double hydroxide: A combined experimental and DFT study. Chem. Eng. J 392:12371

[51] Mei J, Zhang H, Li Z, Ou H (2019) A novel tetraethylenepentamine crosslinked chitosan oligosaccharide hydrogel for total adsorption of Cr (VI). Carbohydr. Polym 224:115154

[52] Liu C, Omer AM, Ouyang X (2018) Adsorptive removal of cationic methylene blue dye using carboxymethyl cellulose/k-carrageenan/activated montmorillonite composite beads: Isotherm and kinetic studies. Int. J. Biol. Macromol 106:823-833